

Theoretical analyses for influences of initial operating parameters on charged-particle transport characteristics in a low-pressure double-wall bounded decaying plasma

Yao-Ting Wang(汪耀庭), Xin-Li Sun(孙鑫礼), Lan-Yue Luo(罗岚月), Zi-Ming Zhang(张子明), He-Ping Li(李和平), Dong-Jun Jiang(姜东君), and Ming-Sheng Zhou(周明胜)

Citation: Chin. Phys. B, 2026, 35 (**8**): 085201. DOI: 10.1088/1674-1056/ae1567
http://cpb.iphy.ac.cn; http://iopscience.iop.org/cpb

What follows is a list of articles you may be interested in

One-dimensional theoretical analysis on charged-particle transports in a decaying plasma with an initial plasma-electrode gap

Xin-Li Sun(孙鑫礼), Yao-Ting Wang(汪耀庭), Lan-Yue Luo(罗岚月), Zi-Ming Zhang(张子明), Meng-Long Zhang(张梦龙), He-Ping Li(李和平), Dong-Jun Jiang(姜东君), and Ming-Sheng Zhou(周明胜)
Chin. Phys. B, 2025, 34 (**11**): 115201. DOI: 10.1088/1674-1056/ade385

Quasi-three-dimensional hydrodynamics of the corona region of laser irradiation of a slab

Xiao-Mei Dong(董晓梅), Ben-Jin Guan(关本金), and Ying-Jun Li(李英骏)
Chin. Phys. B, 2024, 33 (**8**): 085203. DOI: 10.1088/1674-1056/ad4532

Theoretical analyses on the one-dimensional charged particle transport in a decaying plasma under an electrostatic field

Yao-Ting Wang(汪耀庭), Xin-Li Sun(孙鑫礼), Lan-Yue Luo(罗岚月), Zi-Ming Zhang(张子明), He-Ping Li(李和平), Dong-Jun Jiang(姜东君), and Ming-Sheng Zhou(周明胜)
Chin. Phys. B, 2023, 32 (**9**): 095201. DOI: 10.1088/1674-1056/ace033

Analytical model for Rayleigh—Taylor instability in conical target conduction region

Zhong-Yuan Zhu(朱仲源), Yun-Xing Liu(刘云星), Ying-Jun Li(李英骏), and Jie Zhang(张杰)
Chin. Phys. B, 2022, 31 (**10**): 105202. DOI: 10.1088/1674-1056/ac8731

Numerical simulation of the multiple reversed shear Alfvén eigenmodes associated with the triangularity Alfvén gap

Wenjia Wang(王文家), Deng Zhou(周登), Youjun Hu(胡友俊), Yue Ming(明玥), Baolong Hao(郝保龙)
Chin. Phys. B, 2018, 27 (**12**): 125202. DOI: 10.1088/1674-1056/27/12/125202

Theoretical analyses for influences of initial operating parameters on charged-particle transport characteristics in a low-pressure double-wall bounded decaying plasma

Yao-Ting Wang(汪耀庭), Xin-Li Sun(孙鑫礼), Lan-Yue Luo(罗岚月), Zi-Ming Zhang(张子明), He-Ping Li(李和平)†, Dong-Jun Jiang(姜东君), and Ming-Sheng Zhou(周明胜)

Department of Engineering Physics, Tsinghua University, Beijing 100084, *China*

(Received 30 July 2025; revised manuscript received 23 September 2025; accepted manuscript online 21 October 2025)

The influencing mechanisms of the initial operating parameters including the initial plasma density, electron temperature, plasma width, and externally applied voltage on ion extraction characteristics are studied based on a simplified one-dimensional analytical model for a double-wall bounded decaying plasma system. Firstly, a criterion of the dimensionless plasma width ($L_{\min}$) which is normalized with the Debye length for evaluating the state of the sheath expansion is proposed for the first time. Secondly, if the plasma width is larger than the value of $L_{\min}$, a complete sheath expansion process including both the supersonic and subsonic sheath expansion phases occurs during plasma decaying. Consequently, on the one hand, the total ion extraction time and the fraction of the extracted ions at the end of stage II, *i.e.*, the sheath expansion and ion rarefaction wave propagation stage during the whole ion extraction process, can be determined by the initial operating parameters; and on the other hand, it is estimated that about 70% of ions can be extracted at the end of the second stage from the bulk plasma with a consumption of about 62.5% of the total ion extraction time within the parameter ranges studied in this paper. This research is helpful for a deep understanding of the physical mechanisms of the charged-particle transport, as well as for guiding parameter optimizations with better ion extraction performances in practice.

Keywords: ion extraction process, analytical model, parametric analyses

PACS: 52.30.–q, 52.35.Fp, 52.50.Qt, 28.60.+s

DOI: 10.1088/1674-1056/ae1567 **CSTR:** 32038.14.CPB.ae1567

1. Introduction

There are unique features for laboratory or industrial low-temperature plasmas (LTPs). Firstly, most of the laboratory or industrial LTPs are confined in a limited space in contrast to space plasmas, for example, the plasmas exist between electrodes during discharges or near cold walls in materials synthesis or processing. Secondly, except for self-sustaining steady discharges driven by direct-current power supplies,[1] the LTPs may operate under a quasi-steady state with a short period of decaying process driven by alternating-current power supplies (*e.g.*, nano-second pulsed discharges), or even in a continuous decaying process when the external cause is removed (*e.g.*, afterglow plasmas,[2–4] pulsed discharges[5–7] or photoionized plasmas[8–10]). Some representative examples of the laboratory or industrial wall-bounded decaying LTPs include plasma immersion ion implantation (PIII),[11–14] vacuum circuit breaker (VCB),[15–20] and ion extraction from laser-induced plasmas.[21–37] Facing various practical applications of the bounded decaying plasmas (BDPs), from the aspect of fundamental research, there exist complex coupling effects among the spatiotemporal evolutions of the plasma parameters, *e.g.*, number densities and energy distribution functions of species, movement of plasma sheath, electrical potential distributions, and the externally imposed parameters, *e.g.*, nature, temperature, and surface conditions of walls, geometrical configuration of bounded structures, waveforms of applied voltages, which makes the analyses on the physical processes in the BDPs much more difficult. Furthermore, from the aspect of actual applications, the flux of charged particles to the walls, which shows a comprehensive dependence on the foregoing operating parameters of the BDPs, is one of the key factors determining the efficiency and efficacy of applications. For example, the flux and velocity distributions of ions on the target surface are the key parameters influencing the plasma treatment results in PIII;[11] the expansion process of high voltage sheath and the decaying properties of plasma density under the action of the transient recovery voltage determine the turn-off performance of the VCBs;[17,18] and the extraction flux and time of ions are two key parameters for evaluating the performance of the ion extraction process in a laser-induced plasma.[9,21,23] Consequently, it is of great importance to study the influences of various initial operating conditions on the spatiotemporal evolutions of the plasma parameters, especially the spatial variations of the species densities, electric potentials and charged-particle fluxes to the walls with time during plasma decaying.

For the preceding BDP systems, the research is usually focused on the behaviors of the charged particles near the

†Corresponding author. E-mail: liheping@tsinghua.edu.cn

© 2026 Chinese Physical Society and IOP Publishing Ltd. All rights, including for text and data mining, AI training, and similar technologies, are reserved.

cathode surface; that is to say, a single-wall BDP model is employed for studying the sheath expansion process near the cathode and the ion flux to the cathode. For example, the approximate analytical expressions for the ion implantation current on the cathode in both the matrix sheath and Langmuir sheath for the PIII applications were presented firstly by Lieberman,[11] and were modified later for the collisionless matrix sheath by Riemann and Daube[12] with considering the evolutions of the electric field within the sheath during the ion extraction process, and were further extended to formulate flux expressions that accommodate arbitrary initial ion density distributions during the matrix extraction phase by Daube *et al*.[13] In terms of VCBs, Andrew and Varey[15] proposed the continuous transition model based on the assumption of semi-infinite collisionless plasma while with no self-consistently dealing with the plasma attenuation caused by the electrode absorption. With further consideration of the density decaying in the plasma core region located between two negatively biased electrodes, Chen[21] originally established an analytical model after the formation of the Langmuir sheath with considering the balance between the Langmuir flux of the high-voltage sheath and the Bohm flux. Based on Chen's work, the estimation of the ion extraction time under a wide range of the initial plasma density was obtained by Okano;[23] and was further improved with considering the effect of the ion rarefaction wave (IRW) on the ion extraction flux and the sheath movement by Murakami and Nishihara.[24]

Although some important physical processes have been revealed successfully based on the single-wall BDP model, the anode may have non-negligible influences on the decay of the bounded plasmas, which consequently affects the transport of the charged particles, especially for the cases with limited geometrical dimensions, *e.g.*, in the applications of VCBs and ion extraction from laser-induced plasmas.[19,20,27,32,35] For example, in the single-wall BDP model, it is difficult to deal with the oscillation process during the sheath formation process; the IRW propagation process near the anode cannot be included, and consequently, the ion density distribution resulting from the IRW propagation, as well as the ion flux to the anode, also cannot be obtained.[26,27] Therefore, it is necessary to develop a double-wall BDP model to consider the influences of the anode on the sheath formation and the charged-particle fluxes.[26] In recent years, Khrabrov[4] studied the evolution process of the decaying plasmas between two absorbing walls for the case with no externally applied electric fields, and obtained the spatial distributions of the ion density and velocity in the interaction region of two IRWs. Li and his co-workers studied the transport processes of the charged particles in a decaying plasma fully or partially occupying a vacuum gap between two absorbing electrodes for the case with an externally applied electrostatic field, in which the electron motion responding to a suddenly applied electric field was described, and an analytical expression for the oscillation frequency of electrons was presented in Refs. [28,32]; and in particular, a one-dimensional (1D) analytical model has been developed to describe the whole charged-particle transport process with considering the influences of the two absorbing electrodes and the interactions among the solid electrodes, IRWs, and charged particles during plasma decaying under an externally imposed electrostatic field.[35] Although the influences of the initial operating parameters including the externally applied voltage[38–45] and the width of the plasmas[38–41,44] between two electrodes, the initial electron temperature,[27,28,40–42,46] and number density[23,38,40–45,47,48] on the overall ion extraction characteristics have been reported, the influencing mechanisms of the initial operating parameters on the formation of the electrode sheaths, propagation of the IRWs, evolution of the charged particle densities, and fluxes to the walls, as well as the complex interactions between the charged particles and the IRWs in different ion extraction stages starting from the imposing of the external electrostatic field to the disappearance of the plasma, are still very limited. Therefore, the goal of this paper is to reveal the influences of different initial operating parameters, *e.g.*, the initial plasma density, electron temperature, plasma width, and the externally applied voltage, on the physical processes during ion extraction from the double-wall BDPs based on the 1D analytical model developed in Ref. [35], and then, to establish a semi-quantitative relationship between the key parameters, such as the ion extraction flux and the ion extraction time, and the initial operating parameters with the simplification of the original 1D theoretical model.[35] This would be very helpful for presenting a clear physical image of the charged particle transport processes based on the initial operating conditions, and also for providing theoretical guidance for physical design of the ion extraction facilities in actual applications.

2. Derivation of simplified 1D analytical model focusing on influences of initial operating parameters on ion extraction characteristics

2.1. Brief description on the whole ion extraction process and validation of the original 1D analytical model

For the absorbing double-wall BDP system as shown in Fig. 1(a), since the laser-induced plasma initially occupies the space between the two parallel plates uniformly, the two-dimensional (2D) or three-dimensional (3D) effects are not significant; and thus, a 1D model is still used in this paper for revealing the fundamental physical features during the ion extraction process. Therefore, the whole charged particle transport process under an electrostatic field can be divided into three stages based on the original 1D analytical model,[35] *i.e.*, the electron oscillation and matrix sheath extraction stage (stage I), sheath expansion and IRW propagation stage (stage

II), and the plasma collapse stage (stage III). The major features of the foregoing three stages are as follows:

(i) Stage I: Once an electrostatic field is imposed between the two parallel metal electrodes, the matrix sheath near the electrode forms very quickly as a result of the electron oscillations, and its evolution process leads to the formation of the Langmuir sheath at the end of this stage. The ion extraction flux curve during stage I is characterized by a high peak value and a short duration.

(ii) Stage II: The ion extraction flux to the anode is primarily controlled by the IRW propagation, while the ion extraction flux to the cathode is determined by the advancement of the Langmuir sheath with the aid of the IRW propagation. Depending on the relationship between the sheath propagation velocity and the ion acoustic velocity, stage II can be further divided into the supersonic and subsonic propagation phases. In the supersonic propagation phase, the sheath expansion flux is balanced by the Langmuir flux and an additional flux due to the sheath movement; however, in the subsonic propagation phase, the presence of IRW modulates the velocity and density of the ions at the sheath edge and thus changes the corresponding sheath expansion flux. The end of stage II is marked by the disappearance of the IRW at the cathode sheath edge, which originates from the anode.

(iii) Stage III: The sheath expansion flux to the cathode is influenced by the two IRWs coming from the cathode and anode, while the flux to the anode is approximately proportional to t^{-2}, where t is the dimensionless time. Here, it should be emphasized that: firstly, in this paper, the variable with "^" represents the dimensional parameter, while the variable without "^" stands for its corresponding dimensionless form after normalization with the method presented in Ref. [35]; secondly, a normalized form of the equations is used principally for enhancing convenience and clarity in the theoretical analyses, which is more compact than its corresponding dimensional form, remains invariant under changes in the system of units, and facilitates a clear description of the whole ion extraction process.

Except for the preliminary validations of this 1D analytical model by comparing with the particle-in-cell (PIC) modelling results provided in Ref. [35], a further comparison of the model-predicted results with those using the experimental scaling relation, which is obtained by fitting with experimental data,[38] *i.e.*,

$$\frac{\hat{t}_{\rm ext}}{\hat{t}_{\rm ext,ref}} = \left(\frac{\hat{U}_0}{\hat{U}_{0,\rm ref}}\right)^{-0.81} \left(\frac{\hat{L}}{\hat{L}_{\rm ref}}\right)^{1.4} \left(\frac{\hat{n}_0}{\hat{n}_{0,\rm ref}}\right)^{0.56} \tag{1}$$

is conducted in this section, where $\hat{t}_{\rm ext}$, $\hat{U}_0$, $\hat{L}$, and $\hat{n}_0$ stand for the ion extraction time, externally applied voltage, distance between electrodes / plasma width, and the initial plasma number density, respectively. The subscript "ref" indicates the reference case with $\hat{U}_0 = 300$ V, $\hat{L} = 2$ cm, $\hat{n}_0 = 1 \times 10^{16}$ m^{-3}, $\hat{T}_{\rm e,0} = 0.5$ eV, and $M_{\rm i} = 40$ amu.[35] Here, we assume that the initial electron velocity distribution is Maxwellian according to the previous studies, *e.g.*, Refs. [28,29,31,32,35], and thus, an initial electron temperature ($\hat{T}_{\rm e,0}$) can be used. The validity of this assumption is discussed briefly as follows:

(i) During the first stage of the ion extraction process, although the electrons absorb energy from the oscillating electric field, leading to a slight increase in the proportion of highly energetic electrons, the overall electron energy distribution only slightly deviates from the initial Maxwellian distribution.[27,32]

(ii) During the second and third stages, a further deviation from the Maxwellian velocity distribution for electrons occurs since highly energetic electrons are gradually exhausted during the plasma decay process, which results in a decrease of the effective electron temperature and, consequently, leads to a decrease of the ion acoustic velocity. While in the analytical model, the propagation speed of IRW equals that of the initial ion acoustic velocity corresponding to the initial electron temperature, which results in a faster IRW propagation speed and an earlier analytically predicted end time point of the second stage than that of the PIC modeling value. For example, in a typical case studied in Ref. [35], the end time of the second stage predicted by the analytical model is 193.0, while the PIC simulation result is approximately 206.0, with a relative discrepancy of 6.3%.

Based on the preceding discussions, it is seen that the influence of the non-Maxwellian electron velocity distribution during the plasma decay process on the ion extraction characteristics is not significant, and thus, the Maxwellian electron velocity distribution is a relatively good approximation in the 1D analytical model.

Under different values of $\hat{U}_0$, $\hat{L}$, and $\hat{n}_0$, the calculated ratios of $(\hat{t}_{\rm ext}/\hat{t}_{\rm ext,ref})$ using the original 1D analytical model[35] and Eq. (1)[38] are presented in Figs. 1(b)–1(d). It is seen that the theoretically predicted values of $(\hat{t}_{\rm ext}/\hat{t}_{\rm ext,ref})$ are very close to those using the experimental scaling relation with a maximum relative discrepancy of 16.9%. Furthermore, these data are mapped in Fig. 1(e), where each point stands for a specific case in Figs. 1(b)–1(d), and the horizontal axis and vertical axis represent the ion extraction times obtained from Eq. (1), $\hat{t}_{\rm ext,scale}$, and the analytical model, $\hat{t}_{\rm ext,mod}$, respectively.

In Fig. 1(e), the closer the point is to the 45-degree green dashed line, the better the agreement is between the analytical model and the experimental scaling relation. Since the multi-dimensional effects cannot be considered in this 1D analytical model, and there exists a relative error of 15.0% for the scaling relation in Ref. [38], such a level of discrepancy falls within an acceptable range. Consequently, this original 1D analytical

model[35] provides a solid basis for our following derivation on the simplified 1D analytical model in order to reveal the influences of the initial operating parameters on the ion extraction characteristics.

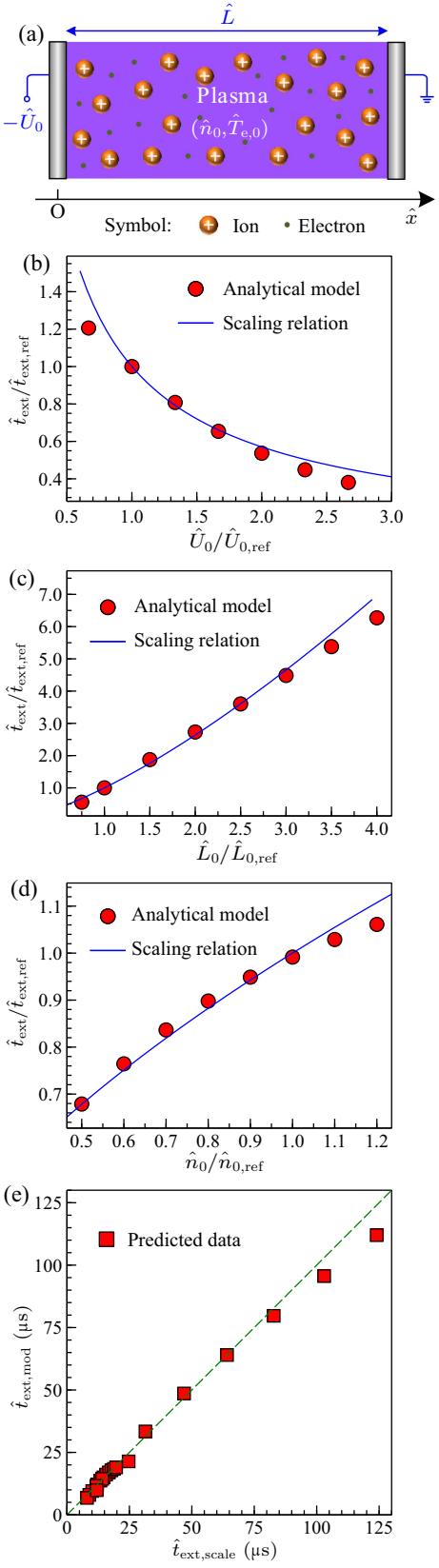


Fig. 1. Schematic diagram of the double-wall BDP system (a), and comparisons of the ion extraction time predicted by the 1D analytical model[35] and experimental scaling relation[38] (b)–(e).

2.2. Simplified 1D analytical model

To clearly reveal the influencing mechanisms of the initial operating parameters on the charged particle transports during plasma decaying, in this section, a simplified 1D analytical model is derived based on the well-established theoretical model as discussed in Subsection 2.1[35] for describing the semi-quantitative relationship between the key parameters of the ion extraction process and the initial operating parameters. For ease of reading, the physical quantities involved in the analytical model are listed in Table 1, and the key parameters in each stage during the ion extraction process are listed in Table 2.

Table 1. Physical quantities involved in the analytical model.

Symbol	Description
$s_{m,ca}/s_{m,an}$	Thickness of the initial matrix sheath near the cathode/anode
$t_{m,end}$	Time point when stage I ends
$s_{sup,end,ca}$	Thickness of the sheath near the cathode when the supersonic sheath expansion phase ends
$t_{sup,end,ca}$	Time point when the supersonic sheath expansion phase ends
$s_{dis,an}$	Thickness of the sheath near the cathode when stage II ends
$t_{dis,an}$	Time point when stage II ends
IRW-A / C	IRW originating from the matrix sheath edge near the anode/cathode

Table 2. Key parameters during each stage.

Stage		Key parameters
Stage I		Γ_{ca}, Γ_{an}, $t_{m,end}$
Stage II	Supersonic	Γ_{ca}, $s_{sup,end,ca}$, $t_{sup,end,ca}$
	Subsonic	$s_{dis,an}$, $t_{dis,an}$, r_2
Stage III		t_{ext}

2.2.1. Analysis on stage I

For stage I, the dimensional thickness of the matrix sheaths in the vicinity of the cathode and anode can be expressed as[35]

$$\hat{s}_{m,ca} = \sqrt{\frac{6\varepsilon_0\hat{U}_0}{e\hat{n}_0}}, \tag{2a}$$

$$\hat{s}_{m,an} = \frac{2}{3}\hat{s}_{m,ca}. \tag{2b}$$

Since the ion extraction fluxes to the cathode and anode can be described by Eqs. (15) and (16) in Ref. [35], by combining those three equations with Eq. (2), it indicates that the ratio of the flux on the cathode to that of the anode in the first stage approximately equals the ratio of the matrix sheath thickness near the corresponding electrodes, *i.e.*,

$$\hat{\Gamma}_{ca}/\hat{\Gamma}_{an} \approx \hat{s}_{m,ca}/\hat{s}_{m,an}. \tag{3}$$

If we take the flux on the cathode as an example to study the influence of the initial operating parameters, it is found

that, in the first stage, the ion extraction flux on the cathode is approximately proportional to the initial plasma number density and the square root of the externally applied voltage, while with no explicit relationship with the plasma width, *i.e.*,

$$\hat{\Gamma}_{\rm ca} \propto \hat{n}_0 \cdot \sqrt{\hat{U}_0}. \tag{4}$$

In addition, the time point when stage I ends can be expressed as

$$t_{\rm m,end} = \sqrt{2\sqrt{1+4\left(\frac{3}{4}s_{\rm m,ca}\right)^{4/3}}-2}. \tag{5}$$

For a typical ion extraction process, a high externally applied voltage (10^3 V$\sim 10^4$ V) is usually employed for a short ion extraction time. Meanwhile, the electron temperature equals the difference between the energy of the laser used for ionization and the ionization energy of the metal atoms, and is usually on the order of 0.1 eV$\sim$1 eV. Therefore, U_0 will be much larger than 1 for the typical ion extraction process, leading to the matrix sheath thickness being much greater than 1. Taking the reference case in Subsection 2.1 as an example, $s_{\rm m,ca} = 60 \gg 1$. Based on the analysis in Appendix A under this condition, equation (5) can be reduced to

$$t_{\rm m,end} \approx 2\left(\frac{3}{4}s_{\rm m,ca}\right)^{1/3} = (6s_{\rm m,ca})^{1/3}, \tag{6}$$

with its corresponding dimensional form as

$$\hat{t}_{\rm m,end} \approx \sqrt{\frac{\varepsilon_0 M_{\rm i}}{\hat{n}_0 e^2}}\left(6\sqrt{\frac{6e\hat{U}_0}{k\hat{T}_{\rm e,0}}}\right)^{1/3} \propto (\hat{n}_0)^{-1/2}\left(\hat{U}_0\right)^{1/6}, \tag{7}$$

where ε_0 is the vacuum permittivity, e is the elementary charge, $M_{\rm i}$ is the ion mass, and k is the Boltzmann constant. From Eq. (7), we can know that the higher the plasma density, the shorter the duration of the first stage; and the higher the applied voltage, the greater the thickness of the matrix sheath, as well as the longer duration time of the first stage; the plasma density has a greater effect on the time duration of the first stage than that of the externally applied voltage.

2.2.2. Analysis on stage II

For stage II, according to our previously established analytical model in Ref. [35], the flux on the anode during this stage is mainly influenced by the IRW and is proportional to the initial plasma density with its dimensional form expressed as

$$\hat{\Gamma}_{\rm an} = \exp(-1)\,\hat{n}_0\sqrt{\frac{k\hat{T}_{\rm e,0}}{M_{\rm i}}}. \tag{8}$$

While the flux evolution on the cathode involves much more complex physical processes, based on the relationship between the sheath propagation velocity and the ion sound velocity, the sheath evolution process near the cathode can be further divided into two phases, *i.e.*, the supersonic and subsonic sheath expansion phases.

(i) **Supersonic sheath expansion phase** During this phase, the Langmuir flux balances with the sheath movement flux, and thus, the evolution of the sheath over time can be analytically solved, *i.e.*,

$$\frac{{\rm d}s}{{\rm d}t} = \frac{4\sqrt{2}}{9}\frac{U_0^{3/2}}{s^2} \to s^3 - s_{\rm m,ca}^3 = \frac{4\sqrt{2}}{3}U_0^{3/2}\left(t - t_{\rm m,end}\right), \tag{9}$$

with its dimensional form written as

$$\frac{\hat{s}^3}{\lambda_{\rm D}^3} - \frac{\hat{s}_{\rm m,ca}^3}{\lambda_{\rm D}^3} = \frac{4\sqrt{2}}{3}\left(\frac{e\hat{U}_0}{k\hat{T}_{\rm e,0}}\right)^{3/2}\omega_{\rm pi}\left(\hat{t} - \hat{t}_{\rm m,end}\right), \tag{10a}$$

$$\hat{s}^3 - \hat{s}_{\rm m,ca}^3 = \frac{4\sqrt{2}}{3}\hat{U}_0^{3/2}\left(\frac{\varepsilon_0}{\hat{n}_0}\right)\left(\frac{1}{eM_{\rm i}}\right)^{1/2}\left(\hat{t} - \hat{t}_{\rm m,end}\right). \tag{10b}$$

The time point, as well as the corresponding sheath thickness, when the supersonic sheath expansion phase ends can be expressed as

$$\frac{{\rm d}s}{{\rm d}t} = 1 \to \begin{cases} t_{\rm sup,end,ca} = t_{\rm m,end} + \frac{3}{4\sqrt{2}U_0^{3/2}}\left(s_{\rm sup,end,ca}^3 - s_{\rm m,ca}^3\right), \\ s_{\rm sup,end,ca} = \sqrt{\frac{4\sqrt{2}}{9}U_0^{3/2}}. \end{cases} \tag{11}$$

Combining Eqs. (2) and (11), if the ratio of the sheath thickness at the end of the supersonic phase to the initial matrix sheath thickness is defined as

$$\begin{aligned} k_{\rm s} &= \frac{s_{\rm sup,end,ca}}{s_{\rm m,ca}} = \frac{\sqrt{\frac{4}{9}\sqrt{2}U_0^{3/2}}}{\sqrt{6U_0}} = \sqrt{\frac{2\sqrt{2}}{27}\sqrt{U_0}} \\ &= \sqrt{\frac{2}{27\sqrt{3}}s_{\rm m,ca}}, \end{aligned} \tag{12}$$

equation (11) can be re-written as

$$t_{\rm sup,end,ca} = t_{\rm m,end} + \frac{9\sqrt{3}}{2}\left(k_{\rm s}^3 - 1\right), \tag{13a}$$

$$s_{\rm sup,end,ca} = k_{\rm s}s_{\rm m,ca}. \tag{13b}$$

As stated in Subsubsection 2.2.1, the values of the externally applied voltage and the initial electron temperature are in the ranges of 10^3 V$\sim 10^4$ V and 0.1 eV$\sim$1 eV, respectively, and the corresponding value of $k_{\rm s}$ ranges from 1.82 to 5.76, which means that the supersonic phase exists with $k_{\rm s} > 1$ under most situations in practice.

By neglecting the matrix sheath thickness since $(k_{\rm s})^3 \gg 1$ for most cases, there exists the following relationship

$$\hat{s}^3 \sim \hat{n}_0^{-1} \to \hat{s} \sim \hat{n}_0^{-1/3}, \tag{14a}$$

$$\hat{s}^3 \sim \hat{U}_0^{3/2} \to \hat{s} \sim \hat{U}_0^{1/2}. \tag{14b}$$

Thus, the relationship among the flux on the cathode and the initial plasma parameters can be expressed as

$$\hat{\Gamma}_{\rm ca} \sim \hat{s}^{-2} \sim \hat{n}_0^{2/3}, \tag{15a}$$

$$\hat{\Gamma}_{\rm ca} \sim \hat{U}_0^{3/2}/\hat{s}^2 \sim \hat{U}_0^{1/2}. \tag{15b}$$

It is seen from Eq. (15) that the initial plasma density has a greater impact on the ion extraction flux to the cathode than that of the externally applied voltage.

(ii) **Subsonic sheath expansion phase** Firstly, the governing equation for the cathode sheath movement in the subsonic phase is

$$\exp(\xi-1)\left(\frac{\mathrm{d}s}{\mathrm{d}t}+1-\xi\right)=\frac{4\sqrt{2}}{9}\frac{U_0^{3/2}}{s^2}, \tag{16a}$$

$$\frac{\mathrm{d}s}{\mathrm{d}t}=\frac{s_0^2}{s^2}\exp(1-\xi)+\xi-1, \tag{16b}$$

with

$$\xi=\frac{s-s_0}{t-t_0},\quad t\geq t_0;\quad s|_{t=t_0}=s_0,\ \ \xi|_{t=t_0}=1, \tag{16c}$$

where s_0 ($=s_{\mathrm{sup,end,ca}}$) represents the starting point of the IRW originating from the cathode side, *i.e.*, IRW-C, at $t_0=t_{\mathrm{sup,end,ca}}$. By introducing the terms $\theta=s/s_0$ and $\tau=(t-t_0)/s_0$, equation (16b) can be re-written as

$$\frac{\mathrm{d}\theta}{\mathrm{d}\tau}=\frac{1}{\theta^2}\exp(1-\xi)+\xi-1, \tag{17a}$$

with

$$\xi=\frac{\theta-1}{\tau},\ \tau\geq 0;\ \ \theta|_{\tau=0}=1,\ \ \xi|_{\tau=0}=1. \tag{17b}$$

Secondly, as stated in Ref. [35], the subsonic phase starts with the excitation of IRW-C, and ends when the IRW starting from the anode side (IRW-A) reaches the cathode sheath edge. Since the propagation of IRW-A can be described by the following equation

$$t=L-s_{\mathrm{m,an}}-x+t_{\mathrm{m,end}}, \tag{18}$$

where x represents the position of the front of IRW-A at time t, the relationship between sheath thickness ($s_{\mathrm{dis,an}}$) and the corresponding time ($t_{\mathrm{dis,an}}$) at the end of stage II can be written as

$$t_{\mathrm{dis,an}}=L-s_{\mathrm{m,an}}-s_{\mathrm{dis,an}}+t_{\mathrm{m,end}}. \tag{19}$$

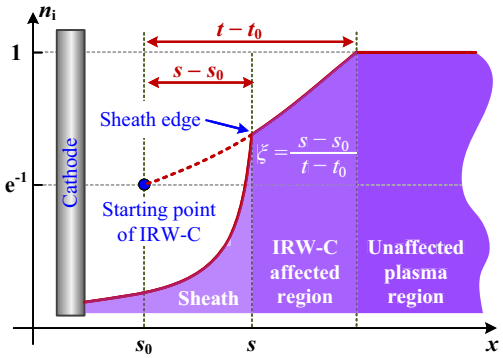


Fig. 2. Illustration of the ion density distribution near the cathode during the subsonic sheath expansion phase.

It is seen from Eqs. (16) and (17) and Fig. 2 that: (i) The variable ξ, ranging from 0 to 1, physically characterizes the relative positions of the cathode sheath edge and the front of IRW-C in the IRW-C affected region. At the moment when the IRW is excited ($t=t_0$ or $\tau=0$) at the position $s=s_0$ or $\theta=1$ near the cathode surface, the value of ξ equals 1. (ii) The moving velocity of the sheath edge ($\mathrm{d}\theta/\mathrm{d}\tau$) gradually decreases with increasing sheath thickness (A detailed analysis can be found in Appendix B). This means that the sheath edge moving velocity approaches zero; and consequently, the sheath position will be stabilized at a certain location. Since the front of IRW-C propagates at the ion acoustic velocity, while the moving velocity of the sheath edge ($\mathrm{d}\theta/\mathrm{d}\tau$) decreases with the increase of the sheath thickness, the sheath position will move farther away from the front of IRW-C after a sufficiently long time, *i.e.*, $\xi\to 0$. (iii) The closer the value of ξ is to zero, the nearer the sheath edge position is to the starting point of IRW-C compared to that of the IRW-C front. Based on the preceding discussions, we can have the following approximated relationship

$$0=\frac{1}{\theta_1^2}\exp(1-0)+0-1\to\theta_1=\exp(1/2). \tag{20}$$

Thus, with the relation $\theta=s/s_0$ and Eq. (20), the cathode sheath thickness at the end of stage II can be expressed as

$$s_{\mathrm{dis,an}}=\exp(1/2)\,s_0=\theta_1 s_0. \tag{21}$$

It should be emphasized that an implicit assumption is employed in deriving Eq. (21), namely, that the sheath needs a sufficiently long time for expansion. In the following, we will discuss the criterion for satisfying this assumption. In order to ensure a sufficiently long sheath expansion time, on the one hand, the IRW-C needs enough propagation time which also makes the relative position of the cathode sheath edge in the IRW-C affected region close enough to the starting point of the IRW-C; on the other hand, a large enough plasma width (L) is necessary to provide the sufficient propagation space and time for the sheath to reach a stable thickness of ($\theta_1 s_0$) as expressed by Eq. (21). Thus, there should exist a minimum plasma width (L_{min}) to satisfy the foregoing requirements with $L\geq L_{\mathrm{min}}$. So, the next step work is to derive the expression for L_{min}.

Firstly, for obtaining an explicit solution of Eq. (17), a simplification is conducted with an approximation of ξ that only contains variable θ or τ, so that the method of separation of variables can be employed. It is seen from Eq. (17) that ξ is inversely proportional to τ, while proportional to θ, and $\xi=\theta=1$ when $\tau=0$. Thus, we hypothesize that ξ has the following approximated form

$$\xi\approx\frac{1}{\tau+1}\approx 2-\theta. \tag{22}$$

Substituting Eq. (22) into Eq. (17), we can have

$$\mathrm{d}\tau = \frac{\theta^2 \mathrm{d}\theta}{\exp(\theta-1)+\theta^2-\theta^3}, \quad (1 \le \theta \le \theta_1). \tag{23}$$

Therefore, the time required for the sheath edge advancing from s_0 to $(\theta_1 s_0)$ can be expressed as

$$\tau_1 = \int_1^{\theta_1} \frac{\theta^2}{\exp(\theta-1)+\theta^2-\theta^3}\mathrm{d}\theta. \tag{24}$$

Doing integration on the right-hand side of Eq. (24) with the aid of a symbolic computing package of Python, Sympy,[49] we can obtain $\tau_1 \approx 2.22$. Consequently, the value of $L_{\min}$ can be determined based on Eq. (19) as

$$\begin{aligned} L_{\min} &= t_0 + \tau_1 s_0 - t_{\mathrm{m,end}} + s_{\mathrm{m,an}} + \theta_1 s_0 \\ &= -\frac{9\sqrt{3}}{2} + \frac{2\sqrt{6}}{3}\sqrt{U_0} + \frac{2}{3}\sqrt[4]{2}\left(\tau_1+\theta_1+\frac{1}{3}\right)\sqrt{U_0^{3/2}} \end{aligned} \tag{25a}$$

for $L = L_{\min}$ at $t_{\mathrm{dis,an}} = t_0 + \theta_1 s_0$. And thus, its corresponding dimensional form can be written as

$$\begin{aligned} \hat{L}_{\min} = &-\frac{9\sqrt{3}}{2}\left(\frac{\varepsilon_0 k \hat{T}_{\mathrm{e},0}}{\hat{n}_0 e^2}\right)^{1/2} + \frac{2\sqrt{6}}{3}\left(\frac{\varepsilon_0 \hat{U}_0}{e\hat{n}_0}\right)^{1/2} \\ &+ \frac{2\sqrt[4]{2}}{9}\left(\tau_1+\theta_1+\frac{1}{3}\right)\left(\frac{\varepsilon_0\hat{U}_0}{e\hat{n}_0}\right)^{1/2}\left(\frac{e\hat{U}_0}{k\hat{T}_{\mathrm{e},0}}\right)^{1/4}. \end{aligned} \tag{25b}$$

So far, for the case with $L \ge L_{\min}$, we have obtained the expressions for the cathode sheath thickness ($s_{\mathrm{dis,an}}$) and the corresponding time point ($t_{\mathrm{dis,an}}$) at the end of the second stage, *i.e.*, Eqs. (21) and (19), respectively. However, when $L < L_{\min}$, the sheath thickness cannot be estimated by Eq. (21). Under such situation, the subsonic cathode sheath movement is described by the following relations based on Eqs. (19) and (23) and the terms $\theta = s/s_0$ and $\tau = (t-t_0)/s_0$, *i.e.*,

$$f(\theta) = \tau = \int_1^{\theta} \frac{\theta^2}{\exp(\theta-1)+\theta^2-\theta^3}\mathrm{d}\theta, \tag{26a}$$

$$\begin{aligned} g(\theta) &= \tau + \theta = f(\theta) + \theta = \frac{L - s_{\mathrm{m,an}} - t_0 + t_{\mathrm{m,end}}}{s_0} \\ &= \zeta. \end{aligned} \tag{26b}$$

Since ζ is determined by the specified initial parameters including the initial plasma density and external potential, equation (26) implies the relationship between ζ and θ as follows:

$$g(\theta) = \zeta \to \theta = g^{-1}(\zeta) = G(\zeta). \tag{27}$$

Doing a polynomial fitting to $G(\zeta)$ based on the solution of Eq. (17), we can get

$$\begin{aligned} \theta \approx G_1(\zeta) = &\ a_0 + a_1\zeta + a_2\zeta^2 + a_3\zeta^3 + a_4\zeta^4 \\ &+ a_5\zeta^5 + a_6\zeta^6, \end{aligned} \tag{28a}$$

with

$$\begin{aligned} &a_0 = 3.72\times10^{-1}, \quad a_1 = 7.62\times10^{-1}, \\ &a_2 = -1.41\times10^{-1}, \quad a_3 = 8.36\times10^{-3}, \\ &a_4 = -2.60\times10^{-3}, \quad a_5 = 9.96\times10^{-4}, \\ &a_6 = -9.80\times10^{-5}. \end{aligned} \tag{28b}$$

Thus, the cathode sheath thickness and the corresponding time when stage II ends can be expressed as

$$s_{\mathrm{dis,an}} = G_1(\zeta)\, s_0, \tag{29a}$$

$$t_{\mathrm{dis,an}} = [\zeta - G_1(\zeta)]\, s_0 + t_0. \tag{29b}$$

In conclusion, the cathode sheath thickness ($s_{\mathrm{dis,an}}$) and the time ($t_{\mathrm{dis,an}}$) corresponding to the end of the second stage can be estimated by Eqs. (19) and (21) for $L \ge L_{\min}$, while by Eq. (29) for the case of $L < L_{\min}$. Taking the case of $\hat{U}_0 = 1500$ V, $\hat{L} = 1.0$ cm ~ 4.0 cm, $\hat{n}_0 = 1\times10^{17}$ m^{-3}, $\hat{T}_{\mathrm{e},0} = 1.0$ eV, $M_{\mathrm{i}} = 235$ amu as an example with the value of $L_{\min} = 2.02$ cm, the comparisons of $s_{\mathrm{dis,an}}$ and $t_{\mathrm{dis,an}}$ by solving Eq. (17) and the corresponding approximated values from Eqs. (19), (21), and (29) are shown in Fig. 3. It is seen clearly that equations (19), (21), and (29) provide a very good approximation for the key parameters, *i.e.*, $s_{\mathrm{dis,an}}$ and $t_{\mathrm{dis,an}}$, during stage II with the maximum relative discrepancies of 0.9% and 0.3%, respectively.

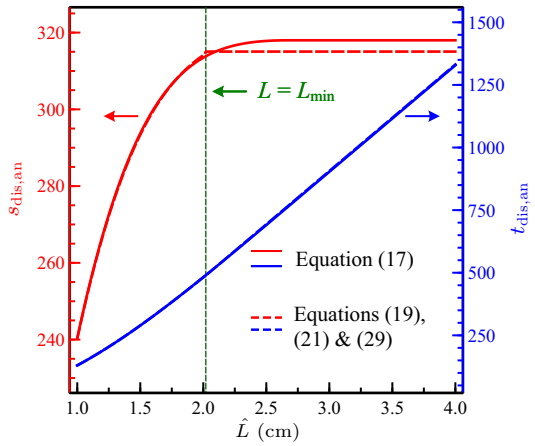


Fig. 3. Comparisons of $s_{\mathrm{dis,an}}$ (red lines) and $t_{\mathrm{dis,an}}$ (blue lines) between the calculated values from the analytical model [Eq. (17)] and the approximated formulas [Eqs. (19), (21) for $L \ge L_{\min}$, and Eq. (29) for $L < L_{\min}$] in stage II.

2.2.3. Analysis on stage III

For the third stage of the ion extraction process, the ion extraction fluxes on the cathode and anode are both rather small. For the ion extraction flux on the cathode, there are generally two states at the end of the second stage. One state is that the Langmuir flux on the cathode equals the Bohm flux. According to the analyses in Subsubsection 2.2.2, the position of the cathode sheath edge is nearly stable at the end of the second stage or the beginning of the third stage for the case of $L \ge L_{\min}$. This also indicates that the Langmuir flux and the Bohm flux are balanced with each other. Consequently, the ion extraction fluxes on the cathode and anode are the same.

Another state is that the Langmuir flux on the cathode is larger than the Bohm flux for the case of $L < L_{\min}$. This means that the cathode sheath expansion is insufficient at the end of the second stage or the beginning of the third stage, under which the Bohm flux is insufficient to balance the Langmuir flux. While for the ion extraction flux on the anode, because the potential difference between the bulk plasma and the anode is almost zero, the ion extraction flux on the anode always equals the Bohm flux during the third stage.

Considering two cases with $\hat{T}_{e,0} = 0.1$ eV and 5.0 eV as those listed in Table 1 of Ref. [27], the corresponding values of L and $L_{\min}$ are 850.77 and 120.32, 1771.03 and 95.92, which correspond to the situations of $L < L_{\min}$ and $L \geq L_{\min}$, respectively. Figure 4 shows the comparisons of the ion extraction fluxes on the anode and cathode for these two cases, where the red and blue lines representing the ion extraction fluxes on the cathode (Γ_{ca}) and anode (Γ_{an}), respectively, are modelling results using the PIC method as reported in Ref. [27]. It is seen clearly that: for the case of $L < L_{\min}$, the simulated flux on the cathode (Γ_{ca}) is higher than that on the anode (Γ_{an}); while for the case of $L \geq L_{\min}$, the simulated values of Γ_{ca} and Γ_{an} are almost the same, and are also close to the calculated results using Eq. (26) in Ref. [35], *i.e.*,

$$\Gamma_{\text{analytical}} = \exp(-1)\left(\frac{t_{\text{dis,an}} - t_{\text{m,end}}}{t - t_{\text{m,end}}}\right)^2. \tag{30}$$

Based on the preceding discussion, the simplified analytical model for describing the 1D ion extraction process bounded between two parallel metal plates under an externally applied electrostatic field is summarized in Table 3.

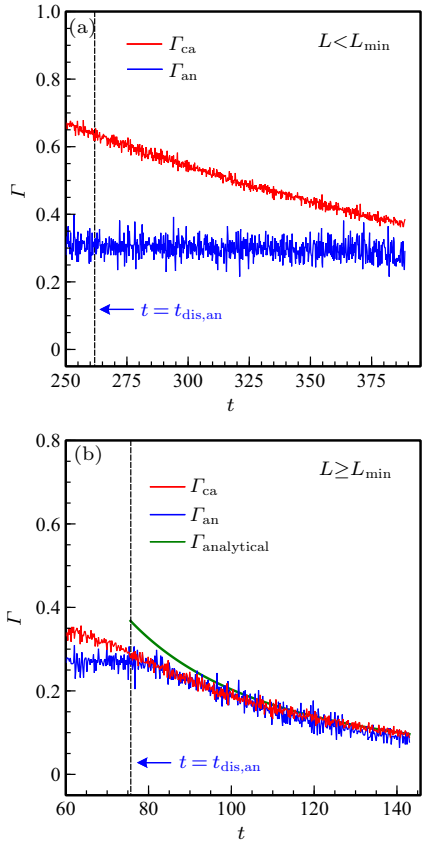


Fig. 4. Comparisons of the ion extraction fluxes on the cathode and anode for the cases of $L < L_{\min}$ (a) and $L \geq L_{\min}$ (b) in stage III.

Table 3. List of the formulas for the simplified 1D analytical model.

Stage No.			Simplified analytical model
Stage I			$\hat{\Gamma}_{ca}/\hat{\Gamma}_{an} \approx \hat{s}_{m,ca}/\hat{s}_{m,an}$, $\hat{\Gamma}_{ca} \propto \hat{n}_0 \cdot \hat{U}_0^{1/2}$, $\hat{t}_{m,end} \propto \hat{n}_0^{-1/2} \cdot \hat{U}_0^{1/6}$
Stage II	Supersonic phase		$\hat{\Gamma}_{ca} \propto \hat{n}_0^{2/3} \cdot \hat{U}_0^{1/2}$
	Subsonic phase	$L \geq L_{\min}$	$s_{dis,an} = \theta_1 s_0$, $t_{dis,an} = L - s_{m,an} - s_{dis,an} + t_{m,end}$
		$L < L_{\min}$	$\zeta = \frac{L - s_{m,an} - t_0 + t_{m,end}}{s_0}$, $s_{dis,an} = G_1(\zeta)\, s_0$, $t_{dis,an} = [\zeta - G_1(\zeta)]\, s_0 + t_0$
Stage III			$\Gamma = \exp(-1)\left[(t_{dis,an} - t_{m,end})/(t - t_{m,end})\right]^2$, $L \geq L_{\min}$

3. Parametric studies on ion extraction characteristics under different initial operating conditions

Based on the derivations in Section 2 and the formulas listed in Table 3, it is seen clearly that there exist strong correlations between the ion extraction characteristics and the initial operating parameters, *e.g.*, the initial plasma density ($\hat{n}_0$) and electron temperature ($\hat{T}_{e,0}$), plasma width or the gap spacing between electrodes ($\hat{L}$) and the externally applied voltage ($\hat{U}_0$) for the specified laser-induced plasmas with the mass of M_i. Thus, the influences of the initial operating conditions on the ion extraction features will be discussed in this section.

In Section 2, the ion extraction features are characterized by the ion extraction flux and its duration time in a complete ion extraction process which includes three stages, *i.e.*, the first stage with the electron oscillation and matrix sheath formation, the second stage with the sheath expansion and IRW propagation, and the third stage with the plasma collapse. Among these three stages, the second stage is more complex and also more important than the other two stages. Based on the discussion in Section 2, there exist three critical values for the plasma width (L), *i.e.*,

$$L_{\text{crt},1} = s_{\text{m,an}} + s_{\text{m,ca}} = \frac{5}{3}\sqrt{6U_0}, \tag{31a}$$

$$L_{\rm crt,2} = s_{\rm m,an} + s_{\rm sup,end,ca} + t_{\rm sup,end,ca} - t_{\rm m,end} = \frac{2}{3}\sqrt{6U_0} + \frac{4}{3}\sqrt{\frac{4\sqrt{2}}{9}U_0^{3/2}} - \frac{9\sqrt{3}}{2}, \tag{31b}$$

$$L_{\rm crt,3} = L_{\rm min} = t_0 + \tau_1 s_0 - t_{\rm m,end} + s_{\rm m,an} + \theta_1 s_0 = -\frac{9\sqrt{3}}{2} + \frac{2\sqrt{6}}{3}\sqrt{U_0} + \frac{2}{3}\sqrt[4]{2}\left(2.22 + \sqrt{e} + \frac{1}{3}\right)\sqrt{U_0^{3/2}}. \tag{31c}$$

Thus, the completeness of the second stage of the ion extraction process can be determined by the following criteria:

(i) $L < L_{\rm crt,1}$: There exists no stage II.

(ii) $L_{\rm crt,1} \le L < L_{\rm crt,2}$: There exists a supersonic sheath expansion phase of stage II.

(iii) $L_{\rm crt,2} \le L < L_{\rm crt,3}$: There exists a complete supersonic sheath expansion phase and part of the subsonic sheath expansion phase approaching a steady cathode sheath edge position of stage II.

(iv) $L \ge L_{\rm crt,3}$: There exist sufficient supersonic and subsonic sheath expansion phases with a steady cathode sheath edge position at the end of stage II.

Here, it should be emphasized that, although the completeness of stage II depends on the initial operating parameters, a complete second stage generally exists in practice. In previous studies, the typical parameter range for the external applied voltage is 10^3 V$\sim 10^4$ V,[22,24,29,30,33,38,40,42,47,48,50] the initial plasma density ranges from 1×10^{16} m^{-3} to 1×10^{17} m^{-3},[27–33,35–38,46] and the initial electron temperature ranges from 0.1 eV to 1 eV.[27–33,35–37,46] Thus, on the one hand, considering the case with the nearly-averaged values of the parameters $\hat{U}_0 = 5000$ V, $\hat{n}_0 = 5\times10^{16}$ m^{-3}, and $\hat{T}_{\rm e,0} = 0.5$ eV, the value of $\hat{L}_{\rm min}$ is 8.2 cm; while on the other hand, if keeping other parameters unchanged, the range of $\hat{L}_{\rm min}$ is 2.5 cm$\sim$13.7 cm when $\hat{U}_0$ changes from 10^3 V to 10^4 V, 18.3 cm$\sim$5.8 cm when $\hat{n}_0$ varies from 1×10^{16} m^{-3} to 1×10^{17} m^{-3}, while 12.1 cm$\sim$6.9 cm with $\hat{T}_{\rm e,0}$ varying from 0.1 eV to 1 eV. In addition, $\hat{L}$ is on the order of 10 cm for a typical ion extraction device.[22,38,50] Therefore, $L \ge L_{\rm min}$ can be satisfied under most cases in practice. Consequently, the characteristics of the ion extraction process including a complete second stage with $L \ge L_{\rm crt,3} = L_{\rm min}$ will be discussed in the following sub-sections.

3.1. Ion extraction ratio at the end of stage II

The previous PIC and analytical studies showed that a large part of ions could be extracted from the main plasma region at the end of stage II.[35] For the case of $L \ge L_{\rm min}$, because a sufficient sheath expansion has been achieved at the end of the second stage with a stable position of the cathode sheath edge, the ratio of the ions extracted from the bulk plasma can be estimated by neglecting the ions in the Langmuir sheath and assuming a uniform ion density distribution in the bulk plasma.[35] Since the plasma density at the sheath edge is approximated as $\exp(-1)$ at the end of stage II, and the distance between the sheath edge and the anode surface is $(L-\theta_1 s_0)$, thus, by neglecting the remaining ions between the sheath edge and the cathode, the ratio of the extracted ions (r_2) can be expressed as

$$r_2 = 1 - \left(1 - \frac{\theta_1 s_0}{L}\right) \times \exp(-1). \tag{32}$$

Letting $k_{\rm L} = L/L_{\rm min}$, we can have

$$r_2 = 1 - \left(1 - \frac{1}{k_{\rm L}}\frac{\theta_1 s_0}{L_{\rm min}}\right) \times \exp(-1) = 1 - \exp(-1)\left[1 - \frac{1}{k_{\rm L}}\frac{\theta_1 s_0}{-9\sqrt{3}/2 + 48^{1/6} s_0^{2/3} + (\tau_1 + \theta_1 + 1/3)\, s_0}\right]$$
$$= 1 - \exp(-1)\left[1 - \frac{1}{k_{\rm L}}\frac{\theta_1}{-9\sqrt{3}/(2s_0) + 48^{1/6} s_0^{-1/3} + (\tau_1 + \theta_1 + 1/3)}\right]. \tag{33}$$

Since s_0 is usually much larger than 1, the above equation can be further simplified as

$$r_2 \approx 1 - \exp(-1)\left[1 - \frac{1}{k_{\rm L}}\frac{\theta_1}{\tau_1 + \theta_1 + 1/3}\right]. \tag{34a}$$

Based on the discussion in Subsubsection 2.2.2, it is known that τ_1 and θ_1 are both constants, *i.e.*, $\tau_1 \approx 2.22$ and $\theta_1 = \exp(1/2)$, while $k_{\rm L}$ is a function of U_0 and L [Eq. (25a)], *i.e.*, $k_{\rm L} = L/L_{\rm min} = k_{\rm L}(U_0, L)$. Therefore, the value of r_2 is determined by the initial operating parameters of U_0 and L, and thus, equation (34a) can be re-expressed as

$$r_2(U_0, L)\, n \approx 1 - \exp(-1)\left[1 - \frac{\theta_1}{\tau_1 + \theta_1 + 1/3}\frac{1}{k_{\rm L}(U_0, L)}\right]. \tag{34b}$$

Considering the real situations during the ion extraction process, *i.e.*, there are some ions in the sheath region, and a parabolic ion density distribution exists in the IRW interaction region, the estimated value of r_2 would be higher than the value predicted by the original analytical model.[35] On the one hand, it can be concluded that, for the critical case of $L = L_{\min}$ ($k_{\rm L} = 1$), the upper bound of the ion extraction ratio at the end of stage II is $r_{2,\rm crt} = 77.6\%$. Taking the critical case ($\hat{U}_0 = 1500$ V, $\hat{L} = 2$ cm, $\hat{n}_0 = 1 \times 10^{17}$ m^{-3}, $\hat{T}_{\rm e,0} = 1.0$ eV, $M_{\rm i} = 235$ amu) with $L = L_{\min}$ as an example, the calculated value of r_2 using the original 1D analytical model is 70.6%, which is lower than $r_{2,\rm crt}$, which, to some extent, validates Eq. (34). On the other hand, for the cases with $L > L_{\min}$, for example, in the case of $\hat{U}_0 = 1000$ V, $\hat{L} = 2$ cm, $\hat{n}_0 = 1 \times 10^{17}$ m^{-3}, $\hat{T}_{\rm e,0} = 1.0$ eV, $M_{\rm i} = 235$ amu with $k_{\rm L} = 1.34$, and the case of $\hat{U}_0 = 1000$ V, $\hat{L} = 2$ cm, $\hat{n}_0 = 2 \times 10^{17}$ m^{-3}, $\hat{T}_{\rm e,0} = 1.0$ eV, $M_{\rm i} = 235$ amu with $k_{\rm L} = 1.89$, the values of r_2 predicted by Eq. (34) are 74.0% and 70.9%, while their counterparts based on the original 1D analytical model are 70.8% and 71.6%, respectively, with the corresponding relative discrepancies of 4.3% and 1.0%. In addition, when the value of $k_{\rm L}$ changes from 1.34 to 2.32 by changing the value of the initial plasma density, the values of r_2 predicted by Eq. (34) also agree well with those predicted by the original 1D analytical model with a maximum relative discrepancy of 4.3%, as shown in Fig. 5. These results further verify the reliability of Eq. (34) for approximately predicting the ion extraction ratio at the end of stage II based on the initial operating parameters.

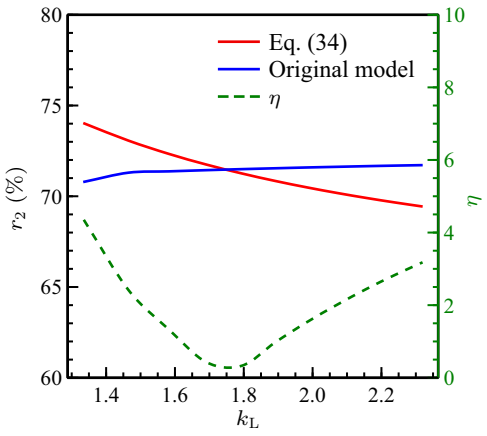


Fig. 5. Comparison of the ion extraction ratios at the end of stage II predicted by Eq. (34) and those of the original analytical model,[35] where η represents the corresponding relative discrepancy.

3.2. Simplified formula for ion extraction time

The integral of the ion extraction flux [Eq. (30)] during the third stage for the case of $L \geq L_{\min}$ can be expressed as

$$\int_{t_{\rm dis,an}}^{t_{\rm ext}} \exp(-1)\left(\frac{t_{\rm dis,an}-t_{\rm m,end}}{t-t_{\rm m,end}}\right)^2 {\rm d}t = \exp(-1)\left[t_{\rm dis,an}-t_{\rm m,end}-\frac{(t_{\rm dis,an}-t_{\rm m,end})^2}{t_{\rm ext}-t_{\rm m,end}}\right]. \quad (35)$$

If the ratio of ions extracted in the third stage is defined as α, the total number of ions extracted is αL, and it is also equal to the integral of the fluxes on the anode and the cathode [Eq. (35)], *i.e.*,

$$2\exp(-1)\left[t_{\rm dis,an}-t_{\rm m,end}-\frac{(t_{\rm dis,an}-t_{\rm m,end})^2}{t_{\rm ext}-t_{\rm m,end}}\right] = \alpha L. \quad (36)$$

Thus, the ion extraction time can be calculated from Eq. (36) as

$$\begin{aligned} t_{\rm ext} &= t_{\rm m,end} + \frac{2(t_{\rm dis,an}-t_{\rm m,end})^2}{2(t_{\rm dis,an}-t_{\rm m,end}) - \exp(1)L\alpha} \\ &\approx \frac{2t_{\rm dis,an}^2}{2t_{\rm dis,an} - \alpha\exp(1)L}. \end{aligned} \quad (37)$$

Based on the analyses in Subsection 3.1, it is known that the proportion of ions extracted at the end of the second stage is about 70%, while the ion extraction time is defined as the time point with 90% of ions extracted from the bulk plasma. Correspondingly, the value of α can be estimated as 0.2, and thus, Eq. (37) can be further simplified as

$$t_{\rm ext} = \frac{10t_{\rm dis,an}}{10-\exp(1)L/t_{\rm dis,an}}, \quad (38a)$$

or

$$\frac{t_{\rm ext}}{t_{\rm dis,an}} = \frac{10}{10-\exp(1)L/t_{\rm dis,an}}. \quad (38b)$$

Based on Eqs. (2), (6), (11), (19), and (21), we can obtain the relationship

$$\begin{aligned} t_{\rm dis,an}(U_0,L) &= L - \sqrt{\frac{4\sqrt{2}}{9}}\theta_1 U_0^{3/4} - \frac{2\sqrt{6}}{3}U_0^{1/2} \\ &\quad + \sqrt{6}U_0^{1/6}, \end{aligned} \quad (39)$$

which indicates that the variable, $t_{\rm dis,an}$, is a function of the initial operating parameters of U_0 and L. Thus, Eq. (38a) can also be re-written as the function of the initial operating parameters of U_0 and L as follows:

$$t_{\rm ext}(U_0,L) = \frac{10t_{\rm dis,an}(U_0,L)}{10-\exp(1)L/t_{\rm dis,an}(U_0,L)}. \quad (40)$$

Letting $\beta = L/t_{\rm dis,an}$, we can estimate the value of β based on Eqs. (19) and (25) as follows:

$$\begin{aligned} 1 < \beta &= \frac{L}{t_{\rm dis,an}} \approx 1 + \frac{s_{\rm m,an}}{t_{\rm dis,an}} + \frac{\theta_1 s_0}{t_{\rm dis,an}} < 1 \\ &\quad + \frac{s_{\rm m,an}}{t_0+\tau_1 s_0} + \frac{\theta_1 s_0}{t_0+\tau_1 s_0} \approx 1.65. \end{aligned} \quad (41)$$

Therefore, the variation range of $(t_{\rm ext}/t_{\rm dis,an})$ can be estimated as

$$1.37 < \frac{t_{\rm ext}}{t_{\rm dis,an}} < 1.81. \quad (42)$$

Taking the case of $\hat{U}_0 = 1000$ V, $\hat{L} = 2$ cm, $\hat{n}_0 = 1 \times 10^{17}$ m^{-3}, $\hat{T}_{\rm e,0} = 1.0$ eV, $M_{\rm i} = 235$ amu with $L > L_{\min}$ as an

example, the predicted dimensionless ion extraction time by Eq. (38) or Eq. (40) is 962.8, while its corresponding value given by the PIC simulation is 992.0. It is seen that Eq. (38) or Eq. (40) provides a very good estimation for the ion extraction time with a relative discrepancy of 3.0%. Similarly, when the value of $k_{\rm L}$ changes from 1.00 to 1.55 by changing the value of the externally applied voltage, the ion extraction times predicted by Eq. (38) or Eq. (40) and those predicted by the original analytical model[35] both increase with a maximum relative discrepancy of 9.5%, as shown in Fig. 6.

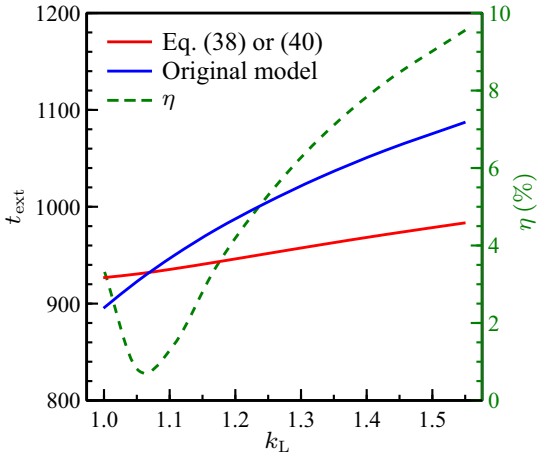


Fig. 6. Comparison of the ion extraction times predicted by Eq. (38) or Eq. (40) and those by the original analytical model,[35] where η represents the corresponding relative discrepancy.

For further validating the reliability of the simplified formula for the ion extraction time, the predicted values of $\hat{t}_{\rm ext}$ by Eq. (38), *i.e.*, $\hat{t}_{\rm ext,simplified}$, are compared with those using the experimental scaling relation (Eq. (1)[38]), *i.e.*, $\hat{t}_{\rm ext,scale}$. It can be seen from Fig. 7 that, among all the values predicted by Eqs. (1) and (38), the relative discrepancies for most cases are no more than 15% with a maximum relative discrepancy of 22.1%. Although the maximum relative discrepancy is a little bit larger than that using the non-simplified analytical model (*i.e.*, 16.9% in Fig. 1(e)[35]), it still falls within an acceptable range while with a simplified relationship for predicting the values of $\hat{t}_{\rm ext}$ according to the initial operating parameters of U_0 and L.

Based on the foregoing analyses, it can be concluded that, in the parameter ranges studied in this paper, the proportion of the extracted ions is about 70% at the end of stage II, while the corresponding time consumption is about 62.5% of the total ion extraction time; that is to say, the extraction of the remaining 20% ions needs to consume 37.5% of the total ion extraction time during the third stage. Therefore, it is necessary to increase the ion extraction ratio or shorten the time duration of stage II for improving the ion extraction performance with the aid of the optimization of the initial operating parameters in future research.

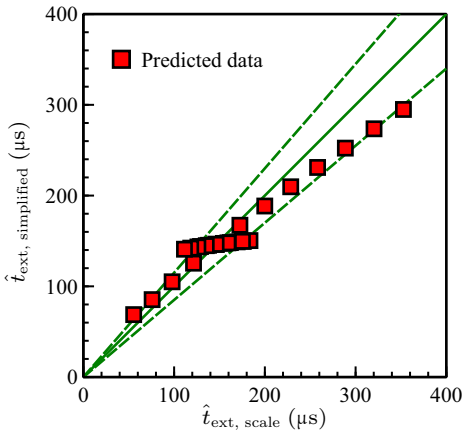


Fig. 7. Comparisons of the ion extraction time predicted by the simplified analytical model [Eq. (38)] and the experimental scaling relation [Eq. (1)] under the initial operating parameter ranges of $M_{\rm i} = 235$ amu, $\hat{T}_{\rm e,0} = 1.0$ eV, $\hat{L} = 4 \sim 15$ cm, $\hat{U}_0 = 0.8 \sim 1.5$ kV, and $\hat{n}_0 = 8 \times 10^{15}$ m^{-3}~1.5×10^{16} m^{-3}. The solid line represents the cases with equal predicted values from Eqs. (1) and (38), while the two dashed lines indicate the upper and lower boundaries with the relative deviations of ±15%.

4. Concluding remarks and future research

In this paper, a simplified 1D analytical model is proposed for revealing the influences of the initial operating parameters, including the initial electron temperature, number density, plasma width, and externally applied voltage, on the characteristics of the ion extraction process. The main conclusions are as follows:

(i) For stage I, the ratio of the ion extraction fluxes on the cathode to that on the anode is almost equal to the ratio of the matrix sheath thickness near the corresponding electrodes. The ion extraction flux to the cathode is approximately proportional to the initial plasma density and the square root of the externally applied voltage, while the duration of the first stage is proportional to $\hat{n}_0^{-1/2}$ and $\hat{U}_0^{1/6}$.

(ii) For stage II, a complete sheath expansion process including both the supersonic and subsonic sheath expansion phases exists when the electrode gap spacing is larger than the critical value of $L_{\rm min}$, which is a function of the initial values of the plasma density, electron temperature, and applied voltage. In the supersonic sheath expansion phase, the ion extraction flux on the cathode is proportional to $\hat{n}_0^{2/3}$ or $\hat{U}_0^{1/2}$; and at the end of stage II with a complete sheath expansion, the fluxes on the anode and cathode are equal to each other in the subsequent stage III.

(iii) For the whole ion extraction process with a complete second stage, both the total ion extraction time and the ion extraction ratio at the end of stage II are determined by the initial operating parameters of U_0 and L, and it is estimated that about 70% of ions have been extracted at the end of the second stage from the bulk plasma with a consumption of about 62.5% of the total ion extraction time within the parameter ranges studied in this paper.

Although the simplified 1D analytical model developed

in this study has been used successfully to predict the characteristics of the ion extraction process based on the initial operating parameters, further optimization needs to be conducted to achieve better performance of the whole ion extraction process with a higher ion extraction flux and a shorter duration of the second stage. In addition, the influences of the vacuum gap between the main plasma region and the electrode surface, the 2D or 3D effects under different electrode configurations, *e.g.*, Π-type or M-type electrode configuration in the ion extraction process, or under even more complex electrode geometries in the fields of plasma immersion ion implantation and vacuum circuit breaker, will be considered in future research for a better understanding of charged particle transport mechanisms in actual applications.

Appendix A

Considering the following function

$$f(x)=\sqrt{2\sqrt{1+4x^{4/3}}-2}\ \text{ with }\ x>0, \tag{A1}$$

it can be re-written as

$$\begin{aligned} f(x)&=\sqrt{2\sqrt{1+4x^{4/3}}-2}=\sqrt{\frac{\left(2\sqrt{1+4x^{4/3}}\right)^2-2^2}{2\sqrt{1+4x^{4/3}}+2}}\\ &=\sqrt{\frac{8x^{4/3}}{\sqrt{1+4x^{4/3}}+1}}=\sqrt{\frac{8x^{2/3}}{\sqrt{x^{-4/3}+4}+x^{-2/3}}}. \end{aligned} \tag{A2}$$

If $x\gg 1$, then we have

$$f(x)\approx g(x)=2x^{1/3}. \tag{A3}$$

Thus, the relative discrepancy between f and g is

$$\eta=\frac{|f(x)-g(x)|}{f(x)}. \tag{A4}$$

Variations of $f(x)$, $g(x)$, and η with x ranging from 10 to 1000 are shown in Fig. A1. It can be seen that, within the range of x considered here, $f(x)$ can be well approximated by $g(x)$. The larger x is, the smaller η is, and the corresponding maximum value of η is 5.4%.

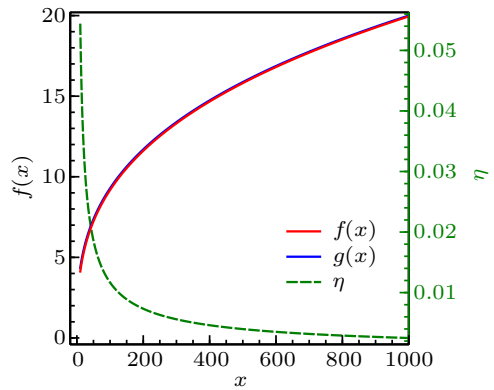


Fig. A1. Comparison of $f(x)$ with $g(x)$ with the corresponding value of η.

Appendix B

Defining the following function from Eq. (17)

$$f(\theta,\tau)=\frac{\mathrm{d}\theta}{\mathrm{d}\tau}=\frac{1}{\theta^2}\exp\left(1-\frac{\theta-1}{\tau}\right)+\frac{\theta-1}{\tau}-1, \tag{B1}$$

and doing the first and second order derivatives with respect to θ on both sides of Eq. (B1), we have

$$\frac{\partial f}{\partial\theta}=-\frac{2\exp\left(1-\frac{\theta-1}{\tau}\right)}{\theta^3}+\frac{1}{\tau}-\frac{\exp\left(1-\frac{\theta-1}{\tau}\right)}{\tau\theta^2}, \tag{B2}$$

$$\frac{\partial^2 f}{\partial\theta^2}=\left(\frac{6}{\theta^4}+\frac{4}{\tau\theta^3}+\frac{1}{\tau^2\theta^2}\right)\exp\left(1-\frac{\theta-1}{\tau}\right). \tag{B3}$$

Since $0<\xi=(\theta-1)/\tau\le 1$, on the one hand, we have $\partial^2 f/\partial\theta^2>0$, which means that the function $(\partial f/\partial\theta)$ always increases with the increase of θ; while on the other hand, with τ going to infinity, θ also goes to infinity, and thus, we can obtain the relationship $\lim_{\tau\to+\infty}(\partial f/\partial\theta)=0$ from Eq. (B2), which means that the value of $(\partial f/\partial\theta)$ is always smaller than zero. Therefore, it can be concluded that the function f always decreases with increasing θ; that is to say, the moving velocity of the sheath edge $(\mathrm{d}\theta/\mathrm{d}\tau)$ decreases with the increase of the sheath thickness.

Acknowledgements

Project supported by the National Key Laboratory Fund form Particle Transport and Separation Technology (Grant No. WZKF-2024-2) and the National Natural Science Foundation of China (Grant No. 11775128).

References

[1] Penning F M 1957 *Electrical Discharges in Gases* (Netherlands: Philips Technical Library)
[2] Couëdel L 2022 *Front. Physics* **10** 1015603
[3] Abuyazid N H, Üner N B, Peyres S M and Sankaran R M 2023 *Nat. Commun.* **14** 6776
[4] Khrabrov A V, Kaganovich I D, Chen J and Guo H 2020 *Phys. Plasmas* **27** 123512
[5] Shao T, Wang R X, Zhang C and Yan P 2018 *High Volt.* **3** 14
[6] Huiskamp T 2020 *Plasma Sources Sci. Technol.* **29** 023002
[7] Wang D Y and Namihira T 2020 *Plasma Sources Sci. Technol.* **29** 023001
[8] Lyon M and Rolston S L 2017 *Rep. Prog. Phys.* **80** 017001
[9] Li H P, Wang P, Wang X, You W, Chai J J and Li Z Y 2015 *High Volt. Eng.* **41** 2825 (in Chinese)
[10] Yang D K, Wang D, Huang Q S, Song Y, Wu J, Li W X, Wang Z S, Tang X H, Xu H X, Liu S and Gui C Q 2022 *Chip* **1** 100019
[11] Lieberman M A 1989 *J. Appl. Phys.* **66** 2926
[12] Riemann K U and Daube T 1999 *J. Appl. Phys.* **86** 1202
[13] Daube T, Meyer P, Riemann K U and Schmitz H 2002 *J. Appl. Phys.* **91** 1787
[14] Israel D, Riemann K U and Tsendin L 2004 *J. Appl. Phys.* **95** 4565
[15] Andrews J G and Varey R H 1971 *Phys. Fluids* **14** 339
[16] Yanabu S, Homma M, Kaneko E and Tamagawa T 1985 *IEEE Trans. Power App. Syst.* **PAS-104** 166
[17] Sarrailh P, Garrigues L, Hagelaar G J M, Sandolache G, Rowe S, Jusselin B and Boeuf J P 2008 *J. Phys. D: Appl. Phys.* **41** 015203

[18] Mo Y P, Shi Z Q, Jia S L and Wang L J 2015 *Phys. Plasmas* **22** 023511
[19] Jia S L, Mo Y P, Shi Z Q, Li J L and Wang L J 2017 *Phys. Plasmas* **24** 103511
[20] Yao X F, Wang J H, Ai S G, Liu Z Y, Geng Y S and Hao Z G 2022 *Engineering* **13** 164
[21] Chen F F 1982 *Phys. Fluids* **25** 2385
[22] Yamada K, Tetsuka T and Deguchi Y 1990 *J. Appl. Phys.* **67** 6734
[23] Okano K 1992 *J. Nucl. Sci. Technol.* **29** 601
[24] Murakami M and Nishihara K 1993 *Phys. Fluids B* **5** 3441
[25] Matsui T, Tsuchida K, Tsuda S, Suzuki K and Shoji T 1996 *Phys. Plasmas* **3** 4367
[26] Litvinov I I 1997 *J. Russ. Laser Res.* **18** 87
[27] Chen J, Fu T Z, Guo H, Li H P, Jiang D J and Zhou M S 2019 *Plasma Sci. Technol.* **21** 045402
[28] Chen J, Li J, Li H P, Jiang D J and Zhou M S 2020 *High Volt. Eng.* **46** 729 (in Chinese)
[29] Chen J, Khrabrov A V, Wang Y T, Li J, Li H P, Jiang D J and Zhou M S 2020 *Plasma Sources Sci. Technol.* **29** 025010
[30] Lu X Y, Yuan C, Zhang X Z and Zhang Z Z 2020 *Chin. Phys. B* **29** 045201
[31] Wang Y T, Chen J, Li H P, Jiang D J and Zhou M S 2021 *Jpn. J. Appl. Phys.* **60** SAAB05
[32] Wang Y T, Luo L Y, Li H P, Jiang D J and Zhou M S 2022 *Acta Phys. Sin.* **71** 232801 (in Chinese)
[33] Singh P, Sridhar G and Maiti N 2023 *IEEE Trans. Plasma Sci.* **51** 35
[34] Singh P, Sridhar G and Maiti N 2023 *Curr. Appl. Phys.* **47** 30
[35] Wang Y T, Sun X L, Luo L Y, Zhang Z M, Li H P, Jiang D J and Zhou M S 2023 *Chin. Phys. B* **32** 095201
[36] Sun J Y, Chen X, Zhao K, Yuan C, Lu X Y, Gao F and Wang Y N 2023 *Plasma Sources Sci. Technol.* **32** 125009
[37] Singh P and Maiti N 2024 *Phys. Scr.* **99** 025609
[38] Yamada K, Tetsuka T and Deguchi Y 1991 *J. Appl. Phys.* **69** 6962
[39] Zhang W X, Cao Z L and Bao C Y 2007 *J. Chin. Mass Spectrom. Soc.* **28** 12 (in Chinese)
[40] Chen J, Xiang J Q, Guo H, Li H P, Chen X, Wang P, Chai J J, Jiang D J and Zhou M S 2017 *High Volt. Eng.* **43** 1830 (in Chinese)
[41] Cao Z L, Zhang W X and Bao C Y 2006 *J. Shenyang Univ. Technol.* **28** 591 (in Chinese)
[42] Xie G F, Wang D W and Ying C T 2005 *Acta Phys. Sin.* **54** 1543 (in Chinese)
[43] Yan M, Wang D W, Ying C T, Zhu X H, Zhu H, Zhang X H, Li J X and Zhang Y X 1997 *Atom. Energy Sci. Technol.* **31** 28 (in Chinese)
[44] Chen J, Liu Z Q, Guo H, Li H P, Jiang D J and Zhou M S 2018 *Acta Phys. Sin.* **67** 182801 (in Chinese)
[45] Ogura K, Kaburaki H and Shibata T 1993 *J. Nucl. Sci. Technol.* **30** 1248
[46] Xiong J G and Wang D W 1999 *J. Tsinghua Univ., Sci. Technol.* **39** 48 (in Chinese)
[47] Hasegawa S, Takei M, Suzuki A and Kurosawa H 2001 *J. Appl. Phys.* **90** 5878
[48] Watanabe J and Okano K 1993 *Phys. Fluids B* **5** 3092
[49] SymPy Development Team, https://docs.sympy.org/latest/index.html [2025-07-29]
[50] Yamada K, Okada H, Tetsuka T and Yoshioka K 1993 *J. Nucl. Sci. Technol.* **30** 143